RAPID COMMUNICATIONS

PHYSICAL REVIEW B VOLUME 39, NUMBER 10 1 APRIL 1989

Photoemission and inverse resonant photoemission studies of $Tl_2Ba_2Ca_2Cu_3O_{10+y}$

H. M. Meyer III, T. J. Wagener, and J. H. Weaver
Department of Materials Science and Chemical Engineering, University of Minnesota, Minneapolis, Minnesota 55455

D. S. Ginley
Sandia National Laboratories, Albuquerque, New Mexico 87185
(Received 28 November 1988)

We present photoemission and inverse photoemission results for single and polycrystalline $Tl_2Ba_{2-x}Ca_{2+x}Cu_3O_{10+y}$. Studies of the occupied states reveal Cu-O and Tl 6*s* hybrid states within ~8 eV of the Fermi level E_F. Tl 4*f* emission characteristic of a single chemical environment, the Cu $2p_{3/2}$ main line and satellites, complex O 1*s* emission derived from chemically inequivalent oxygen sites, and Ca and Ba emission reflecting Ca-Ba disorder within the unit cell were observed. Inverse photoemission results show a low density of states within ~1 eV of E_F and structure at ~3, ~7, 9.6, and 14 eV above E_F that is associated with Tl 6*p*, Ba 5*d*, Ca 3*d*, and Ba 4*f* empty levels. Resonant inverse photoemission highlights the O 2*p* holes near E_F. Differences and similarities to $Bi_2Ca_{1+x}Sr_{2-x}Cu_2O_{8+y}$ are discussed.

The recent addition of the Tl-Ba-Ca family of copper-oxide-based superconductors[1] to the already long list of high-T_c materials is stimulating spectroscopy studies of the electronic states of these materials.[2–8] The goal of such studies is the discovery of distinct signatures that can be linked to the superconducting transition temperature, on the one hand, and the use of electronic structures to characterize other properties of these unique materials, on the other.

In this paper, we present x-ray photoemission (XPS) and inverse photoemission (IPES) results for bulk ceramic and single-crystal $Tl_{2-x}Ba_{2+x}Ca_2Cu_3O_{10+y}$, abbreviated Tl-Ba-Ca-Cu-O herein. Core-level and valence-band results obtained with XPS allow direct comparison with ground-state band calculations and make it possible to identify effects due to second phases present in single-crystal and polycrystalline samples. IPES results obtained with a range of incident electron energies reveal unoccupied electronic state features within 17 eV of the Fermi level E_F. Resonant IPES techniques highlight the O 2*p*-derived holes above E_F.

Bulk ceramic $Tl_{2-x}Ba_2Ca_2Cu_3O_y$ was synthesized from a stoichiometric mixture of dry CuO, BaO, CaO, and Tl_2O_3 that was ground and sieved. 15 g of the mixed powder was pressed in a die at 24000 psi for 7 min. The resulting pellet was then sintered in air at 850 °C on Pt for 15 min. It was then crushed, reground, sieved (No. 50 mesh), and repressed. The pellet was resintered in air at 850 °C for 15 min. The pellet was then oxygen annealed for 12 h at 850 °C with a 5-h slow cool under oxygen. The resulting material was primarily $Tl_{2-x}Ba_2Ca_2Cu_3O_y$ and had zero resistance greater than 118 K.

Single crystals were grown from the melt by a pseudo-flux growth technique. CuO, CaO, BaO, and Tl_2O were mixed in a 2:1:2:0.5 ratio and ground and sieved (No. 50 mesh). The powder was loaded into a 1-in. Pt crucible tightly sealed with a Pt lid. The crucible was placed in a vertical tube furnace under flowing O_2, and the temperature was rapidly brought to 900 °C (5 min), then to 950 °C (30 min), held there for 60 min, cooled to 700 °C in 12.5 h, and then to room temperature in another 3 h. The crystals were mechanically extracted and then oxygen annealed for 12 h at 850 °C with 5-h slow cool.[9]

The samples for investigation were mounted on copper posts with conducting silver epoxy and inserted into the vacuum system in preparation for *in situ* fracturing. As will be discussed below, the fractured surfaces of the bulk ceramic were of lower quality than the single crystals, as judged from grain-boundary-related spectral features. Surfaces obtained by scraping the fractured surface *in situ* with a diamond file showed substantially reduced contamination, as has been reported by others for Cu-O-based superconductors.[8] Single crystals of approximate dimension $1\times1\times0.1$ mm^3 were also mounted onto copper posts and were covered with beads of epoxy. Prior to study, the epoxy was broken off to expose internal surfaces of the crystal. *In situ* optical microscopy revealed a high density of surface steps and terraces. No time dependencies were observed that could be related to sample degradation or oxygen loss at 300 K.

The samples were fractured or cleaved at 300 K immediately before measurements were undertaken. XPS studies were done at an operating pressure of 5×10^{-11} Torr. The x-ray photon energy was 1486.6 eV and the energy resolution of the spectrometer was 0.6 eV (see Ref. 10 for a detailed description). Inverse photoemission studies were performed in a four-chamber system optimized for photon energies of 10–44 eV. It contains a Pierce-type electron gun from Kimball Physics that produces a collimated 1×5 mm^2 electron beam, an $f/3.5$ grating in a near-normal-incidence monochromator geometry, and a position-sensitive detector.[10]

Figure 1 shows the occupied and unoccupied electronic states for the bulk ceramic from 12 eV below to 17 eV above E_F. The broad structure centered ~4 eV below E_F with a shoulder at 2.5 eV is similar to what has been observed for semiconducting and superconducting forms of the 1:2:3 and 2:1:4 copper oxides and for $Bi_2Ca_{1+x}Sr_{2-x}$-

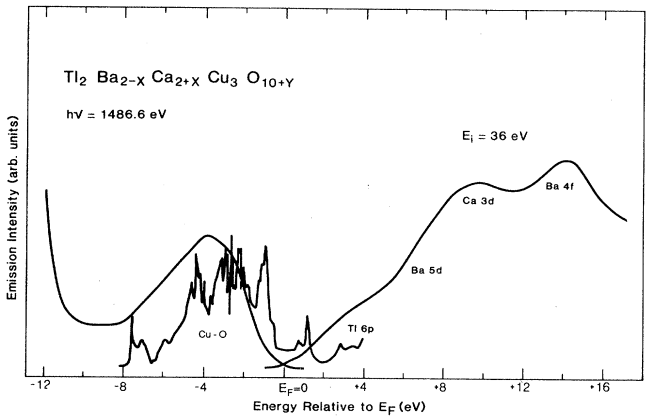

FIG. 1. Occupied electronic states for $Tl_2Ba_{2-x}Ca_{2+x}Cu_3O_{10+x}$ obtained with XPS, empty states obtained with IPES, and the density of states, DOS, from Ref. 5. The importance of final-state effects is seen by the $\sim$1.5-eV shift in centroid of the calculated and experimental Cu-O–derived states. The metallic nature of the material is evident from the Fermi-level cutoff. Empty-state structures are identified in terms of the dominant character of the bands.

Cu_2O_{8+y}, abbreviated Bi-Ca-Sr-Cu-O (see Refs. 8, 11, 12 and citations therein). This indicates that the valence-band photoemission features are dominated by Cu-O derived features. Comparison with Bi-Ca-Sr-Cu-O shows additional emission near 7 eV and a less distinct Fermi level cutoff. The Cu satellite structure associated with the d^8 final-state configuration was not observed because of overlapping Ba $5p$ and Tl $5d$ emission; it has been identified in synchrotron radiation studies that used Cu $3p$-$3d$ resonant photoemission.[2] The results of Fig. 1 also reveal a feature at $\sim$9 eV that is reminiscent of the 9.5-eV structure observed for the 2:1:4's and 1:2:3's. The intensity of this weak feature did not change with time. Although its origin remains controversial, it has been associated with final-state effects involving oxygen.[13,14] Recent resonant photoemission studies have shown that this feature resonates at the onset of O $2s$ excitations.[15]

Comparison of the experimental results to the one-electron density of states[4,5] again indicates the importance of final-state effects for the Cu-O–derived hybrid states (Fig. 1). As for the other Cu-O–based superconductors, the calculations predict that the centroid of the occupied levels would lie $\sim$1.5 eV closer to the Fermi level than is observed experimentally. The calculations indicate that states at E_F arise primarily from Cu $3d$–O $2p$ hybrids, with one band crossing E_F for each Cu-O sheet for Tl-Ba-Ca-Cu-O (3 total).[4–7] While the calculations point to many features common to the Tl and Bi systems, there are also differences, including negligible contributions of Tl $6p$–O $2p$ states at E_F compared to Bi $6p$–O $2p$.[5,7] This probably explains the less-pronounced Fermi-level cutoff for Tl-Ba-Ca-Cu-O compared to Bi-Ca-Sr-Cu-O. Calculations predict the importance of Tl $6s$–O $2p$ mixing for Tl-Ba-Ca-Cu-O, an effect not observed for Bi-Ca-Sr-Cu-O because the Bi $6s$ levels fell $\sim$11.3 eV below E_F.[4,5] It is likely that the shoulder at $\sim$7 eV reveals an admixture of Tl $6s$ states. Direct superposition of XPS spectra for Bi-Ca-Sr-Cu-O and Tl-Ba-Ca-Cu-O shows somewhat higher overall emission in this energy region, probably because of the Tl $6s$ emission. We also note that Tl may contribute some $6s$ character at E_F, as pointed out by Sleight.[16] (Sleight has also cautioned that band calculations have so far been based on structures which differ from the observed structure.)

In Fig. 1 the empty states from 0 to 17 eV above E_F are revealed by the photon distribution curve (PDC) measured for an incident electron energy of 36 eV. The empty state PDC is scaled to give the same step at E_F as for the occupied states, solely for convenience. The PDC exhibits low emission to $\sim$1 eV, shoulders at $\sim$3 and $\sim$7 eV, and maxima at 9.6 and 14 eV. From the band calculations, we associate the states near the Fermi level with the uppermost Cu-O hybrids, with increasing Tl $6p$ character at higher energy. Comparison with equivalent spectra for Bi-Ca-Sr-Cu-O shows significant Bi $6p$ character centered $\sim$4 eV above E_F with Bi-O hybrid bands that reach the Fermi level.[17] We associate the structure at $\sim$7 eV with Ba $5d$ character, by analogy to results for $YBa_2Cu_3O_{7-x}$ (Ref. 18) and from E_i-dependent inverse photoemission results which show that the Ba $5d$ states are enhanced for $E_i = 29$ eV due to the $5p$-$5d$ giant dipole resonance.[17] The Ba $4f$ emission at 14 eV is more atomic in character and its photon emission cross section is enhanced for increasing E_i.[19] In the future, it will be a guidepost of the chemical state of Ba, and we note it appears shifted by 4.7 eV relative to Ba metal.[20] The maximum at 9.6 eV is related to Ca $3d$ states. This identification can readily be made with resonant inverse photoemission when E_i is scanned through the Ca $3p$ core-level threshold and the delayed $3p$-$3d$ giant dipole resonance is observed at $E_i \sim 40$ eV.[17] In these E_i-dependent studies, two constant photon-energy features are also observed at 20.2 and 12.5 eV. They result from the radiative decay of plasmons, as discussed for $YBa_2Cu_3O_{7-x}$ (plasmon energy 22.2 eV) and $Bi_2Ca_{1+x}Sr_{2-x}Cu_2O_{8+y}$ (21.2 and 15 eV).[17]

To examine the distribution of O $2p$ hole states, we also undertook resonant inverse photoemission studies of the bulk ceramic in the region of the O $2s$ core threshold.[17] Normalized PDC's for E_i between 14 and 21 eV are shown at the left of Fig. 2. Examination shows enhancement that reaches a maximum around $E_i = 18$ eV. To be quantitative, we show selected inverse constant-final-state-energy (ICFS) spectra at the right of Fig. 2. They were obtained by determining the emission intensity in a step-by-step manner for final-state energies $E_f = 0$, 0.5, . . . ,4 eV from the normalized PDC's. There is clear enhancement over background for each final-state energy, and the shape of that structure suggests decomposition into two components, as drawn. One occurs when E_i sweeps through $\sim$18 eV (solid line). This is due to incident-electron excitation of O $2s$ core electrons into O $2p$ holes, followed by radiative decay, i.e., O $(2s^1 2p^6) \rightarrow$ O $(2s^2 2p^5) + h\nu$. This photon emission couples with the continuum decay channels of inverse photoemission to produce resonantly enhanced emission.[21] Another way of displaying these results is given in the inset of Fig. 2 where the areas under the curves are plotted

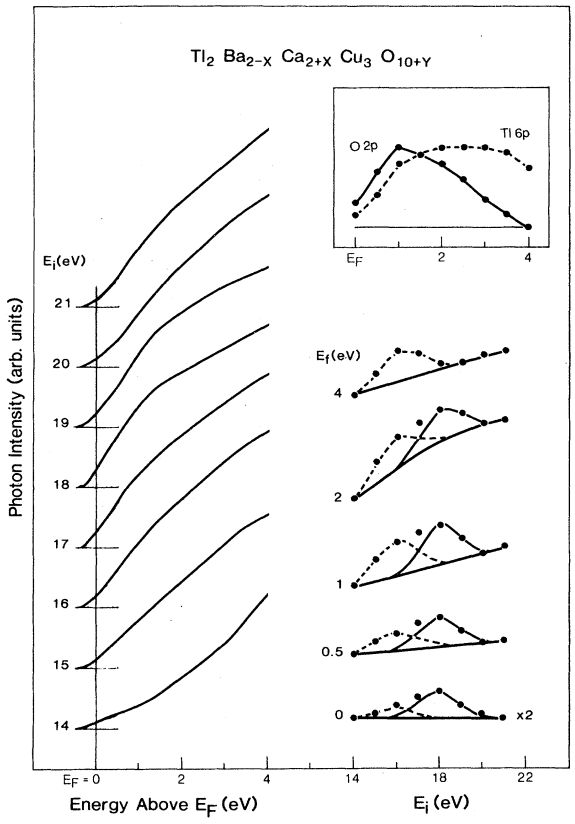

FIG. 2. Left panel: PDC's for $Tl_2Ba_{2-x}Ca_{2+x}Cu_3O_{10+x}$ for $E_i = 14$–21 eV, normalized to electron dose to emphasize enhancement related to O $2s$–O $2p$ resonant IPES excitations. Right: Inverse constant final-state energy spectra derived from the PDC's for final states at 0, 0.5, 1, 2, and 4 eV above E_F quantitatively show enhancement for E_i's centered around 18 eV for O $2s$-$2p$ excitation and 16 eV for Tl $5d$-$6p$ excitation. Inset: Distribution of O $2p$ holes and the Tl $6p$ states, as determined by the areas under the constant final-state energy curves.

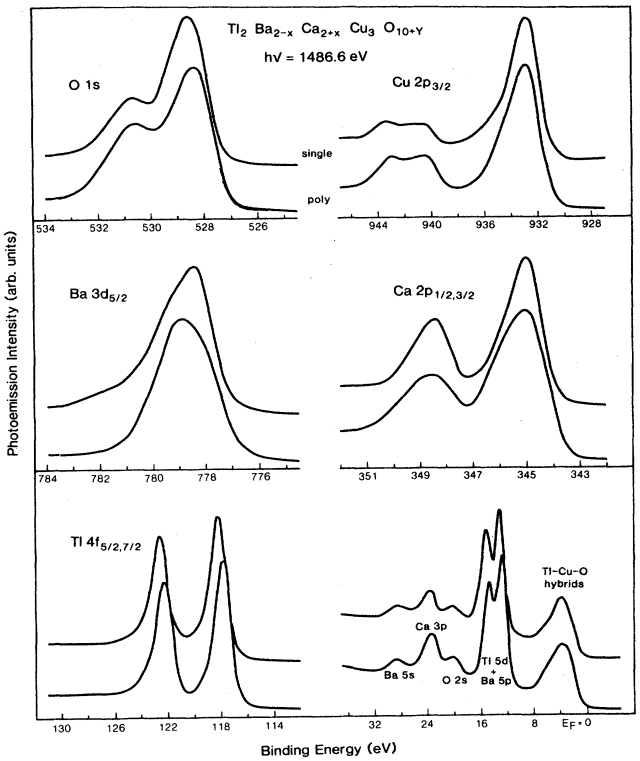

FIG. 3. Core-level spectra for single and polycrystalline $Tl_2Ba_{2-x}Ca_{2+x}Cu_3O_{10+y}$ showing complex O $1s$ bonding at 528 eV and second-phase contribution at 531 eV, the Cu $2p_{3/2}$ main line and satellites, multiple configurations for Ba and Ca, and a single bonding configuration for Tl with an asymmetry associated with an energy-loss feature.

for the different final-state energies, i.e., energies relative to the Fermi level. As such, this is a direct measure of the distribution of O $2p$ holes. A similar distribution of holes was found for Y-Ba-Cu-O and Bi-Ca-Sr-Cu-O (Ref. 17) and these results agree with x-ray absorption and electron-energy-loss experiments for Y-Ba-Cu-O.[22,23]

The results of Fig. 2 also reveal enhancement for $E_i = 16$ eV for all final states shown. We associate this enhancement with the Tl $6p$ states since it occurs near the Tl $5d$ threshold. The results shown in the inset suggest that these empty Tl $6p$ levels come close to E_F and are distributed upward, consistent with Fig. 1.

In Fig. 3 we show core-level and valence-band results for Tl-Ba-Ca-Cu-O. For both single-crystal and polycrystalline samples, we find two O $1s$ features with the main peak at 529 eV and a shoulder at ~531 eV. The O $1s$ data for Tl-Ba-Ca-Cu-O are consistent with the O $1s$ results obtained for Bi-Ca-Sr-Cu-O (Refs. 12 and 24) and can be described as follows. The main peak is made up of three types of lattice oxygen atoms, namely oxygen atoms bonded to Ba and Ca (lowest-binding-energy component), oxygen atoms bonded in Cu-O planes (as well as oxygen atoms bonded between Cu-O and Tl-O planes), and oxygen atoms bonded in Tl-O planes (highest-binding-energy component). A fourth feature at ~530 eV is also observed. For the 1:2:3's and 2:1:4's, we suggested that it was due to contributions from the $d^9\underline{L}$ ground state while Fujimori *et al.*[24] suggested that it was an energy-loss feature. Tl $4f$ line-shape analysis for Tl-Ba-Ca-Cu-O, analogous to the Bi $4f$ analysis in Bi-Ca-Sr-Cu-O in Ref. 24, indicates the presence of a plasmon loss feature shifted ~1.1 eV to higher binding energy. With further consideration of the screening argument of Wendin,[21] we suspect that the origin of the fourth O $1s$ component is due to energy-loss features. Unfortunately, overlap with the large feature at 531 eV for the present results frustrates quantitative analysis of the O loss intensity.

For the polycrystalline samples, the O $1s$ feature at 531 eV undoubtedly reflects second-phase material in grain boundaries, equivalent to that observed in Ba-containing 1:2:3's.[11] O $1s$ spectra from polycrystalline Bi-Ca-Sr-Cu-O, which is Ba-free, show much reduced emission at 531 eV and it is negligible for the single crystals reported to date.[12,24] Our polycrystalline Tl-Ba-Ca-Cu-O samples that were fractured showed a much larger 531-eV peak but subsequent scraping reduced the amount of contamination. For the single-crystal results, we associate the

531-eV feature with impurities exposed during cleaving, a process which would preferentially occur at weak spots in the crystal. These conclusions are consistent with what has been observed for single and polycrystalline[25] $YBa_2Cu_3O_{7-x}$.

The upper-right panel of Fig. 3 shows the Cu $2p_{3/2}$ core-level emission. Both sample types exhibit a main line and a complex satellite structure at higher binding energy, features that reflect the Cu^{2+} bonding configuration as discussed extensively elsewhere.[26] For the polycrystalline samples, the satellite-to-main-line intensity ratio (0.38) and main-line full width at half maximum (FWHM, 2.9 eV) are nearly the same as for $Bi_2Ca_{1+x}Sr_{2-x}Cu_2O_{8+y}$, $La_{1.85}Sr_{0.15}CuO_4$, and $YBa_2Cu_3O_{7-x}$. However, Tl-Ba-Ca-Cu-O single crystals exhibit reduced satellite emission (satellite/main intensity ratio = 0.21) and main-line width (2.4 eV), possibly because of the nature of the exposed surface.

The Ba $3d_{5/2}$ core-level emission shown in Fig. 3 exhibits two components for both sample types, one centered at 778.3 and the other at 779.2 eV and each having a FWHM of 1.5 eV.[27] The Ca $2p$ spectra also are derived from two components, although less obviously so, especially for the single-crystal sample. To fit the Ca spectra we used two spin-orbit-split pairs separated by ~ 1 eV (splitting 3.5 eV, branching ratio 2, FWHM 1.35 eV).[28] We attribute these high and low binding-energy components for both Ba and Ca to Ca-Ba disorder within the unit cell. This disorder involves sites between Tl-O and Cu-O sheets or between adjacent Cu-O sheets and the bonding configurations (charge distribution) differ substantially. Analogous conclusions have been reached for Sr and Ca in Bi-Ca-Sr-Cu-O.[29]

The Tl $4f_{5/2,7/2}$ core-level emission for the polycrystalline sample is located at 117.8 and 122.2 eV, shifted 0.4 eV to lower binding energy relative to the single crystal. Line-shape analysis shows that these sharp features also have energy-loss features associated with them, as noted above. Attempts to fit the experimental line shapes were unsuccessful if only an asymmetry due to metallic screening was included, but the results could be fitted very well with a component shifted 1.1 eV and an asymmetry parameter of zero (negligible metallic screening). From the shallow Tl $5d$ level, there is also a 0.4-eV binding-energy shift, although overlap with Ba $5p$ emission complicates analysis. The origin of the binding-energy difference is not known, although we speculate that it may be related to oxygen stoichiometry. Similar differences have been reported for Y-Ba-Cu-O with changes in oxygen content.[25] Finally, in Fig. 3 we show that the shallow core and valence-band region extending to 36 eV below E_F shows the Ba $5s$ (28.5 eV), Ca $3p$ (23.5 eV), and O $2s$ (20.2 eV) emission, along with overlapping Tl $5d$ and Ba $5p$ emission.

The work at the University of Minnesota was supported by the Office of Naval Research and U.S. Defense Advanced Research Projects Agency. The work at Sandia National Laboratories was supported, in part, by the Department of Energy, Office of Basic Energy Sciences, under Contract No. DE-AC04-76DP00789. The technical support of R. J. Baughman and M. A. Mitchell is gratefully acknowledged.

[1]Z. Z. Sheng and A. M. Herman, Nature (London) **333**, 55 (1988).

[2]R. L. Stockbauer *et al.*, *High-T_c Superconducting Thin Films, Devices, and Characterizations—1988,* edited by G. Margaritondo, M. Onellion, and R. Joynt, Proceedings of the American Vacuum Society Special Conference on High-Temperature Superconductivity (AIP, New York, in press).

[3]R. V. Kasowski, W. Y. Hsu, and F. Herman, Phys. Rev. B **38**, 6420 (1988).

[4]A. J. Freeman, S. Massidda, and J. Yu, in *Chemistry of High Temperature Superconductors II,* edited by D. L. Nelson and T. F. George, ACS Symposium Series, No. 377 (American Chemical Society, Washington, DC, 1988).

[5]P. Marksteiner *et al.*, Phys. Rev. B (to be published).

[6]B. A. Richert and R. E. Allen, in Ref. 2.

[7]B. A. Richert and R. E. Allen (unpublished).

[8]P. Steiner *et al.*, (unpublished).

[9]D. S. Ginley *et al.*, J. Crystal Growth **91**, 456 (1988).

[10]S. A. Chambers *et al.*, Phys. Rev. B **35**, 634 (1988); Y. Gao *et al.*, J. Phys. E **21**, 489 (1988).

[11]H. M. Meyer III *et al.*, Phys. Rev. B **38**, 6500 (1988).

[12]H. M. Meyer III *et al.*, Phys. Rev. B **38**, 7144 (1988).

[13]M. Onellion *et al.*, Phys. Rev. B **38**, 881 (1988).

[14]D. Ramaker, Phys. Rev. B **38**, 11816 (1988).

[15]R. L. Kurtz *et al.*, Phys. Rev. B **39**, 4768 (1989).

[16]A. W. Sleight, Science **242**, 1519 (1988).

[17]T. J. Wagener *et al.*, Phys. Rev. B **39**, 2928 (1989).

[18]T. J. Wagener *et al.*, Phys. Rev. B **36**, 3899 (1987).

[19]Y. Gao *et al.*, Phys. Rev. B **36**, 3971 (1987); Th. Fauster and F. J. Himpsel, *ibid.* **30**, 1874 (1984).

[20]J. Knaski and P. O. Nilsson, J. Phys. F **11**, 1859 (1981).

[21]G. Wendin, Phys. Scr. (to be published); and (private communication).

[22]N. Nücker *et al.*, Phys. Rev. B **37**, 5158 (1988).

[23]P. Kuiper *et al.*, Phys. Rev. B **38**, 6483 (1988).

[24]A. Fujimori *et al.*, Phys. Rev. B **39**, 2255 (1989).

[25]H. M. Meyer III *et al.*, J. Appl. Phys. (to be published).

[26]G. van der Laan *et al.*, Phys. Rev. **23**, 4369 (1981).

[27]A third component at higher binding energy was needed to fit both spectra. It is attributed to emission from second phases [$\sim 12\%$ (7%) of total intensity for polycrystalline (single) samples and centered at 780.8 eV].

[28]A third pair (intensity 11%) was required to fit the data for polycrystalline Tl-Ba-Ca-Cu-O and is attributed to grain-boundary phases.

[29]S. Kohiki *et al.*, Phys. Rev. B **38**, 7051 (1988).